Chemistry–A European Journal
Research Article
doi.org/10.1002/chem.202301099
Chemistry Europe
European Chemical Societies Publishing
www.chemeurj.org

Hot Paper

Unexpected Reduction of a Coordinated Diazapyridinophane Ligand Bound to Chromium(III) Ion Leading to Delocalization of the Unpaired Electron across Two Isolated Pyridine Units

Kristin Krämer,[a] Markus Schmitz,[a] Harald Kelm,[a] Christoph van Wüllen,[b] and Hans-Jörg Krüger*[a]

Dedicated to Dr. Hartmut Spiering on occasion of his 80th birthday.

In the tetraazamacrocyclic ligand *N,N'*-dimethyl-2,11-diaza-[3.3](2,6)pyridinophane (L-N_4Me_2), the two pyridine units are separated from each other by sp^3-hybridized triatomic bridges. Such electronically isolated pyridine moieties are considerably less prone to reductions than di- or triimines. A detailed structural, magnetic, and spectroscopic investigation of the complexes $[Cr(L\text{-}N_4Me_2)(OAc)_2]$ and $[Cr(L\text{-}N_4Me_2)(OAc)_2](PF_6)$, in combination with theoretical calculations, reveals that the reduced complex must be described as a chromium(III) ion coordinated to the anionic radical ligand $(L\text{-}N_4Me_2)^{\bullet-}$ rather than a low-spin chromium(II) ion bound to closed-shell ligands. Thus, it is, to the best of our knowledge, only the second example of a stable and structurally characterized metal complex containing a reduced isolated pyridine unit. The stability is attributed to the delocalization of the unpaired electron across the two pyridine units, mediated by their interaction to the metal ion.

Introduction

Tri- and tetraazamacrocyclic ligands are frequently used with metal ions to create highly stable coordination moieties with specific coordination environments imposed onto the metal ion by the particular structural features of the macrocycle. Furthermore, certain coordination sites on the metal ion can be designed in such a way that they are easily accessible for the interaction with a substrate, while others are protected by the macrocyclic ligand.[1] When discussing the reactivity of such complexes, it is essential to know whether such a macrocyclic ligand could be involved as a redox-active unit in the reactions being studied. Azamacrocyclic ligands with ligand backbones containing only aliphatic saturated carbon chains and tertiary amine donor functions are, to best of our knowledge, not known to be involved in any redox activity in complexes. Uncoordinated pyridine can only be reduced at potentials well below −2.4 V versus the saturated calomel electrode.[2] Thus, provided that strongly electron-withdrawing substituents on a pyridine ring are absent and pyridine moieties are not part of a π-conjugated diimine system, macrocyclic ligands containing electronically isolated pyridine units can safely be considered redox-inactive in solvents commonly used for investigating metal complexes, such as acetonitrile. This property of such a macrocycle is usually regarded as valid even in the coordinated state despite the fact that coordination of the metal cation is expected to increase the redox potential of the pyridine moiety, possibly to such an extent that this premise might no longer hold. An example for macrocyclic ligands which contain electronically isolated pyridine units is the ligand *N,N'*-dimethyl-2,11-diaza-[3.3](2,6)pyridinophane (L-N_4Me_2), which is depicted in Scheme 1. This twelve-membered macrocyclic ligand features two pyridine units, which are separated from each other by sp^3-hybridized *tri*atomic $-CH_2-N(CH_3)-CH_2-$ bridges. The uncoordinated ligand does not exhibit any reduction within the

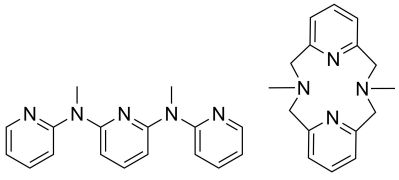

ddpd **L-N_4Me_2**

Scheme 1. Ligand ddpd and L-N_4Me_2.

[a] *K. Krämer, Dr. M. Schmitz, Dr. H. Kelm, Prof. Dr. H.-J. Krüger*
RPTU Kaiserslautern-Landau
Department of Chemistry
Erwin-Schrödinger Straße 54, 67663 Kaiserslautern (Germany)
E-mail: krueger.hj@chem.rptu.de

[b] *Prof. Dr. C. van Wüllen*
RPTU Kaiserslautern-Landau
Department of Chemistry and Forschungszentrum OPTIMAS
Erwin-Schrödinger Straße 54, 67663 Kaiserslautern (Germany)

Supporting information for this article is available on the WWW under https://doi.org/10.1002/chem.202301099

accessible potential range of acetonitrile (see also Figure S11 in the Supporting Information). Derivatives of this ligand have been used, for example, in functional biomimetic model studies,[3] in investigations of complexes with spin-crossover or valence tautomeric properties,[4] and in reaction studies of complexes containing metal ions in low oxidation states.[5] In all these complexes no redox activity of the coordinated macrocyclic ligand has been demonstrated.

For a general discussion of the properties of such complexes, it is, however, crucial to know whether or not the coordinated macrocyclic ligand can always be considered redox innocent. We, therefore, initiated an investigation to test the redox activity of the coordinated macrocyclic ligand L-N_4Me_2 in reduced chromium complexes because the chemistry of chromium(II) ions, in particular, is characterized by their pronounced reducing power.[6]

In a groundbreaking publication, Wieghardt et al. could unambiguously demonstrate by structural and spectroscopic methods as well as by theoretical calculations that, for a series of chromium complexes with derivatized reduced tris(2,2′-bipyridyl) ligands $[Cr(^tbipy)_3]^n$ (with $n = 0, 1+, 2+$; ^{t}bipy = 4,4′-di(*tert.*-butyl)-2,2′-bipyridine), the chromium ion is not reduced to oxidation states from +II down to 0 for an increasing number of electrons. Instead the electronic structure was determined to have arisen from a chromium(III) ion and, depending on *n*, one to three coordinated radical anion ligands $(^tbipy)^{\bullet-}$.[7] Subsequently, analogous descriptions of such an electronic structure were reported for other reduced chromium complexes in which radical ligands derive from potentially reducible neutral ligands. These ligands typically contain multiple nitrogen donor atoms participating in a conjugated π-molecular orbital system, for example aliphatic and aromatic diimines or triimines.[8,9]

In contrast, if the ligand is non-reducible and the ligand field strength is sufficiently high, for example ligands with carbon or phosphor donor atoms, the relatively rare low-spin chromium(II) state can be achieved.[9] Recently, Heinze et al. reported on a redox pair of an octahedral chromium complex generated from the coordination of two units of the tridentate ligand *N*,*N*′-dimethyl-*N*,*N*′-dipyridine-2-yl-pyridine-2,6-diamine (ddpd, Scheme 1).[10,11] This ligand contains three pyridine moieties which are electronically separated from each other by sp^3-hybridized amine nitrogen atom bridges. The two complexes $[Cr(ddpd)_2]^n$ ($n = 3+, 2+$) were characterized by structural, magnetochemical, and UV-Vis spectroscopic data in combination with quantum chemical calculations. The reduced complex (n = 2+) was identified as a low-spin chromium(II) complex capable of a temperature-induced spin crossover transition. The observed redox-inactivity of ddpd is most likely linked to the presence of the electron-donating amine substituents, which seem to lower the redox potential of the coordinated ligand sufficiently to warrant the formation of a chromium(II) complex. This reasoning is supported by the observation that replacing the amine nitrogen bridges by sp^3-hybridized carbon bridges reduces the electron-donating capabilities of the pyridine substituents, thereby increasing the redox potential of the coordinated pyridine unit. Thus, theoretical calculations on the electronic nature of the analogous dicationic complex $[Cr(bpmp)_2]^{2+}$ containing two 2,6-bis(2-pyridylmethyl)pyridine ligand units (bpmp) instead of the ddpd ligands already attribute a certain admixture of a state arising from a chromium(III) ion antiferromagnetically coupled to a ligand-centered radical to a low-spin chromium(II) state.[12a] In a further study using the tridentate ligand tris(2-pyridyl)ethane (tpe), Heinze et al. concluded, after comparing the experimental electronic absorption spectrum of an electrochemically generated solution of the chromium complex $[Cr(tpe)_2]^{2+}$ with the electronic absorption spectrum obtained by theoretical calculations, that this complex is best described as a chromium(III) ion coordinated to a $(tpe)^{\bullet-}$ radical ligand.[12b] The latter complex was not isolated as a solid, and no further spectroscopic characterization of this complex is available.

Considering the range of possible electronic ground states in these reported complexes,[10–12] an investigation of chromium complexes containing the macrocyclic ligand L-N_4Me_2 was initiated. Similar to the ddpd, bpmp and tpe ligands, the tetraazamacrocyclic ligand L-N_4Me_2 also consists of electronically isolated pyridine units, which are, however, separated from each other by sp^3-hybridized triatomic bridges instead of a single atom bridge. The electron-donating properties of the pyridine substituents in L-N_4Me_2 are similar to those in bpmp and tpe, but lower than those in ddpd. In this study, *cis*-bis(acetato)chromium complexes containing the L-N_4Me_2 ligand were investigated. We discovered that our experimental findings of the reduced complex are more compatible with a ligand-based instead of a metal-based reduction, leading to a chromium(III) ion coordinated to a monoanionic radical macrocycle rather than a low-spin chromium(II) ion bound to a neutral macrocyclic ligand.

Results and Discussion

The synthesis of the chromium complexes with L-N_4Me_2 starts with the reaction of chromium(II) acetate and the tetraazamacrocyclic ligand in acetonitrile solution (Scheme 2). Ether diffusion into the reaction solution affords deep green crystals whose chemical analysis is consistent with the composition $[Cr(L\text{-}N_4Me_2)(OAc)_2]$ (**1**).[13] The substance displays a pronounced sensitivity towards oxygen in solution, resulting in an almost immediate colour change from green to brown. The solid crystalline compound can be handled briefly in air, but color changes will occur over time even in the solid state. The cyclic voltammogram of **1** displays a reversible oxidation at −1.10 V

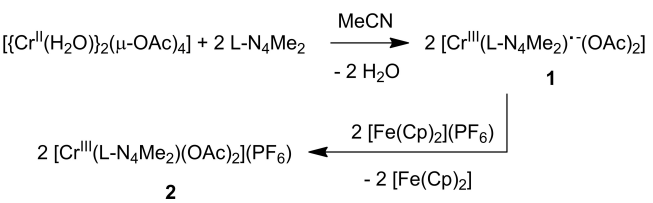

Scheme 2. Preparation of compounds **1** and **2**.

vs. SCE (−1.55 V vs. Fc/Fc^+). A cyclic voltammogram of the reverse reaction, the reduction starting with the corresponding oxidized complex $\mathbf{1}^+$, is shown in Figure S10.[13] To establish the electronic nature of **1**, a suitable complex with a well-defined electronic ground state was necessary. Therefore, in addition to **1**, the corresponding blue bis(acetato)chromium(III) complex $[Cr(L\text{-}N_4Me_2)(OAc)_2](PF_6)$ (**2**) containing the neutral macrocyclic ligand was prepared by oxidizing **1** with one equivalent of ferrocenium hexafluorophosphate (Scheme 2).

Using a SQUID magnetometer, the magnetic properties of both solids were investigated in a temperature range between 2 and 300 K. The temperature dependence of the product $\chi_M{\cdot}T$ of the molar magnetic susceptibility χ_M and the temperature T at an applied magnetic field of 0.5 T is shown in Figure 1. The data have been corrected for the occurrence of a temperature-independent paramagnetism. For **2**, the $\chi_M{\cdot}T$-curve starts with a value of 1.86 cm^3Kmol^{-1} at 2 K, increases to a value of 1.95 cm^3Kmol^{-1} at 7 K, and then remains constant at higher temperatures. The observed value of 1.95 cm^3Kmol^{-1} and the absence of a pronounced zero-field splitting are typical for the $S=3/2$ spin arising from an octahedral chromium(III) ion. For **1**, a $\chi_M{\cdot}T$-value of 0.52 cm^3Kmol^{-1} is found at 2 K, which raises to 1.02 cm^3Kmol^{-1} at 37 K and stays almost constant over the entire higher temperature range. At low temperatures a zero-field splitting constant $|D|$ of 3.44 cm^{-1} was determined. The measured $\chi_M{\cdot}T$-value of 1.02 cm^3Kmol^{-1} indicates the presence of an $S=1$ spin system, thereby, ruling out the description of complex **1** as a high-spin chromium(II) complex.

The observed spin state of $S=1$ could be attributed either to a low-spin chromium(II) complex or, alternatively, to a chromium(III) ion ($S_{Cr}=3/2$) exhibiting a strong antiferromagnetic exchange coupling to a radical ligand ($S_{rad}=1/2$). The ligand donor environment in **1** speaks against the first interpretation; the ligand field strength of a N_4O_2-ligand sphere is not expected to be large enough to warrant a low-spin state of a chromium(II) ion.[14] Assuming the latter interpretation to be correct, the absolute value of the exchange coupling constant $|J|$ between the chromium(III) ion and the radical ligand (using a Heisenberg-Dirac-van Vleck magnetic exchange interaction Hamiltonian ($\widehat{H} = -2J\vec{S}_1\cdot\vec{S}_2$) must be larger than 250 cm^{-1} to replicate the experimentally observed magnetic data (Figure S6).[13] Although unprecedented until now, the only possible ligand unit in **1**, which could sustain a reduction to form a stable coordinated π-radical ligand, is the macrocyclic ligand.

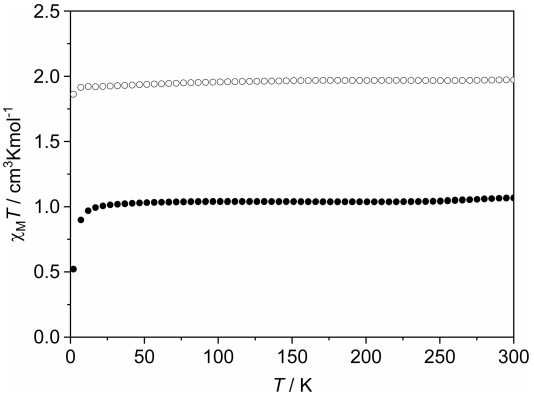

Figure 1. Temperature-dependence of $\chi_M T$ for **1** (●) and **2** (○) between 2 and 300 K measured at an applied magnetic field of 0.5 T.

Structural determinations were carried out for both compounds at 150 K. A perspective view of complex **1** is presented in Figure 2. The complex cation $\mathbf{1}^+$ in **2** possesses an analogous overall structure. A comparison between some selected bond lengths is provided in Table 1. In both complexes, the macrocyclic ligand reveals the typical tetradentate coordination mode of $L\text{-}N_4Me_2$, resulting in a distorted *cis*-octahedral N_4O_2-coordination environment around the chromium ions. Thus, the diazapyridinophane ligand is folded along the N_{amine}—N_{amine}-axis, leaving two coordination sites *trans* to the pyridine units to be filled by the two monodentate acetate ligands. The two N_{py} and

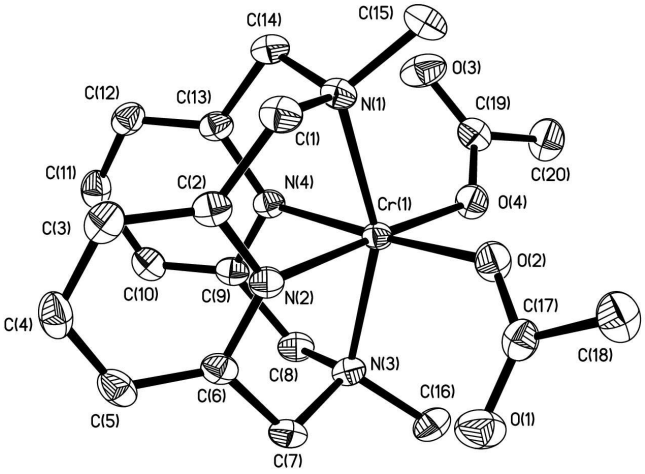

Figure 2. Perspective view of complex **1** with thermal ellipsoids displaying a probability level of 50%. The hydrogen atoms are omitted in the drawing for the sake of clarity. The same atom numbering scheme is applied to the complex cation $\mathbf{1}^+$ in **2** as it is to complex **1**.

Table 1. Selected experimental[a] and calculated[b] bond lengths (in Å) in **1** and **2**. Selected bond angles are additionally listed in Table S2.[13]

	experimental		calculated	
	1 [150 K]	**2** [150 K]	**1**	$\mathbf{1}^+$
$Cr–N_{amine}$	2.152(1), 2.155(1)	2.134(2), 2.142(2)	2.208	2.201
$Cr–N_{py}$	1.965(1), 1.978(1)	1.998(1), 2.014(1)	2.004	2.054
$Cr–O_{OAc}$	1.985(1), 1.998(1)	1.930(1), 1.938(1)	1.979	1.931
C–N	1.359(2), 1.364(2) 1.365(2), 1.365(2)	1.337(2), 1.341(2) 1.339(2), 1.341(2)	1.356	1.336
$C–C_{adj}$	1.375(3), 1.378(3) 1.374(3), 1.374(3)	1.379(2), 1.380(2) 1.383(3), 1.386(3)	1.380	1.387
$C–C_{dis}$	1.386(3), 1.396(3) 1.394(3), 1.394(3)	1.384(3), 1.386(3) 1.384(3), 1.386(3)	1.399	1.391

[a] The equivalent bonds Cr-N(1) and Cr-N(3) are summarized as $Cr–N_{amine}$; Cr–N(2) and Cr–N(4) as $Cr–N_{py}$; Cr–O(2) and Cr–O(4) as $Cr–O_{OAc}$; C(2)–N(2), C(6)–N(2), C(9)–N(4) and C(13)–N(4) as C–N; C(2)–C(3), C(5)–C(6), C(9)–C(10) and C(12)–C(13) as $C–C_{adj}$; C(3)–C(4), C(4)–C(5), C(10)–C(11) and C(11)–C(12) as $C–C_{dis}$. [b] Density functional calculations were performed using the program package *Turbomole*,[16] applying the B3LYP[17] functional in combination with the def2-TZVP[18] basis set.

the two O donor atoms form, together with the chromium ion, an almost ideal equatorial plane.[15] The *idealized* symmetry of the complex fragment [Cr(L-N_4Me_2)] is C_{2v}; due to the particular coordination modes of the two acetate ligands, this symmetry is reduced to C_2 for the entire complex.

The average lengths of the Cr–O, Cr–N_{py}, and Cr–N_{amine} bonds in $\mathbf{1}^+$ are 1.934, 2.006, and 2.138 Å, respectively, and serve as a reference for a chromium(III) ion bound to a neutral tetraazamacrocyclic ligand. In addition, the C–N bonds and the C–C bonds adjacent (C–C_{adj}) and distant (C–C_{dis}) to the C–N bonds average to 1.340, 1.382, and 1.385 Å, respectively. These bond lengths are typical for a coordinated 2,6-disubstituted neutral pyridine unit. Upon reduction, the Cr–N_{py} bonds decrease in their average length by 0.034 Å to 1.972 Å, while the Cr–O and Cr–N_{amine} bonds increase in length by 0.058 and 0.016 Å to 1.992 and 2.154 Å, respectively. These changes are interpreted as an indication of the reduction of the ligand L-N_4Me_2 to a monoanionic radical ligand (L-N_4Me_2)$^{\bullet-}$ in **1**. The negative charge on the pyridine moiety strengthens the σ-donor properties of this coordination unit, affording shorter Cr–N_{py} bonds. The considerable increase of the Cr–O bond length can be attributed to a stronger *trans* influence of the macrocyclic ligand when it is a stronger σ-donor in its monoanionic oxidation state. The rather modest decrease in length of the axial Cr–N_{amine} bonds results from slight readjustments of the macrocyclic ring system due to the movement of the chromium ion into the macrocyclic cavity when the Cr–N_{py} bonds decrease in length. The reduction of the pyridine units in **1** is also reflected by the bond lengths within the rings compared to those found in $\mathbf{1}^+$. Thus, especially, the average length of the C–N bonds increases by 0.023 Å to 1.363 Å. In contrast, the C–C_{adj} bonds shorten by merely 0.007 Å, and the C–C_{dis} bonds marginally increase in size by just 0.008 Å. These changes are similar to those reported in a genuine pyridine radical complex where a *single* anionic 4-*tert*-butylpyridine radical ligand (C–N: +0.022 Å, C–C_{adj}: −0.013 Å and C–C_{dis}: +0.009 Å) was coordinated to a high-spin (β-diketiminato)(4-*tert*-butylpyridine)iron(II) fragment.[19,20] A similar degree of shortening of the Cr–N bonds has been reported for chromium(III) complexes containing a single reduced bipyridine ligand.[7]

The $S=1$ spin state of complex **1** could, in principle, also arise from a low-spin [Cr^{II}(L-N_4Me_2)$(OAc)_2$] species. In this case, the decrease of the Cr–N_{py} bond lengths upon reduction of $\mathbf{1}^+$ to **1** should instead be attributed to a strengthening of the π-back bonding due to the presence of the more electron-rich low-spin chromium(II) ion in **1**. Such an explanation for the shorter Cr–N_{py} bonds in **1** is analogous to that used for the observation that the Ru^{II}–N bonds are almost as long as the Ru^{III}–N bonds in $[Ru(bipy)_3]^{2+/3+}$ complexes.[21] However, we consider this interpretation to be less likely due to the considerably weaker π-acceptor strength of an electronically isolated pyridine ligand compared to a bipyridine ligand.

Additional support for the assignment of complex **1** as [Cr^{III}(L-N_4Me_2)$^{\bullet-}(OAc)_2$] is provided by density functional (DFT) calculations employing the B3LYP[17] functional and def2-TZVP[18] basis sets. Geometry-optimization calculations, subjected to the condition that a $S=1$ state is prevalent in the neutral complex, yield a chromium(III) ion coordinated to a monoanionic macrocyclic ligand. Spin density plots of both the reduced and oxidized calculated complexes (Figure 3) show a cube-like shape of the positive spin density at the chromium(III) ion due to the presence of a t_{2g}^3 electron configuration. In the reduced complex, there is, in addition, the presence of a negative spin density located on the π-systems of the two pyridine rings of the ligand.

As generally observed in calculations concerning metal complexes with the diazapyridinophane ligand, the metal-nitrogen bond lengths are slightly overestimated. But an inspection of the bond lengths between the oxidized and the reduced complexes (see Table 1) shows that the theoretical results compare very well with the experimentally observed trends, especially the increase in Cr–N_{py} bond lengths upon oxidation of **1**.[22]

The pattern of bond length changes in the pyridine rings is also well reproduced. The calculated changes in lengths of the C–N, C–C_{adj}, and C–C_{dis} bonds of −0.020, +0.007 and −0.008 Å upon the oxidation of **1** to $\mathbf{1}^+$ agree perfectly with the experimentally determined structural changes of −0.023, +0.007, and −0.008 Å, respectively. The larger change in the

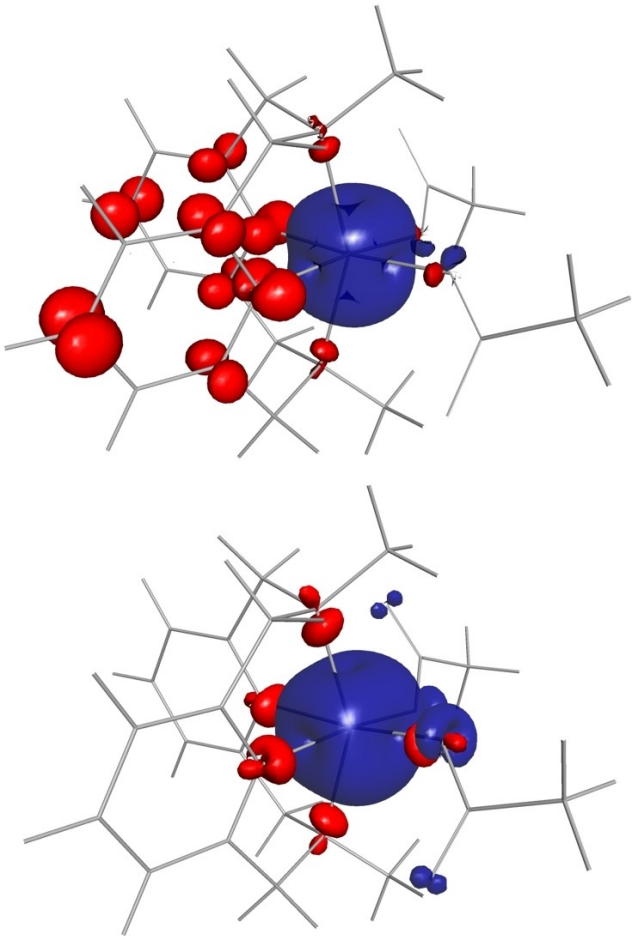

Figure 3. Perspective views of the calculated spin densities (contour value = 0.007 e Å^{-3}) in **1** (top) and $\mathbf{1}^+$ (bottom).

length of the C–N bonds upon reduction of the complex is explained by the larger orbital contribution of these three atoms on the pyridine ring to the calculated highest occupied molecular orbital (HOMO) leading to π-antibonding interaction (see also plot of HOMO (β-spin) in Figure 5). These contributions of the atomic orbitals to the HOMO are also reflected in the spin density plot displayed in Figure 3. Although this congruence in structural properties already provides a convincing argument for the validity of the theoretical calculations in assigning the electronic nature of **1**, a comparison of other experimental properties of **1** and $\mathbf{1}^+$ with those obtained from calculations is needed to increase confidence in the correctness of the calculations. Therefore, the investigation was extended to the UV-Vis-NIR and IR spectroscopic properties of the complexes in solution.

Conductivity measurements of 1 mM solutions of compound **1** and **2** in acetonitrile result in values for Λ_M of 16.5 (23.1 °C) and 116.6 $\Omega^{-1}\cdot cm^2\cdot mol^{-1}$ (22.3 °C), respectively. This finding indicates that neither **1** nor $\mathbf{1}^+$ undergo extensive ligand substitution reactions with the solvent and that the structural compositions found in the solid state are retained in solution. Thus, all spectroscopic properties determined for the complexes in solution should also apply to their solid states.

The magnetic properties of **1** in deuterated acetonitrile solution was investigated by Evans' method.[23] At a temperature of 293 K a $\chi_M \cdot T$-value of 1.12 $cm^3 Kmol^{-1}$ was found, which is consistent with the magnetic data in the solid state.

The electronic absorption spectra of **1** and $\mathbf{1}^+$ in acetonitrile solutions recorded at room temperature under anaerobic conditions are shown in Figure 4. The corresponding absorption data are listed in Table S3.[13] In addition, using TD-DFT methods, the electronic absorptions were calculated for **1** and $\mathbf{1}^+$.[13] The results of the theoretical calculations are inserted as bar charts onto the graphs of the experimental spectra where the heights of the bars illustrate the relative dipole oscillator strengths of the calculated transitions. The agreement between the calculated and the experimental spectra is reasonable to good, considering that the time-dependent DFT calculations tend to exhibit larger deviations in the excitation energies when they concern charge transfer transitions.[24] But, even more importantly, if the correlation between experimental and calculated spectra is reasonable, the calculations allow an assignment of the absorption bands. They show, that if the electronic excitations concern the ligands, either the π-molecular orbitals of pyridine rings (py) of the ligand L-N_4Me_2 or the π-molecular orbitals of the carboxylate units (O_2C) of the acetate ligands are involved (Figure S21 and S22).[13]

In the visible range, the oxidized complex mainly displays two moderately intense absorptions with maxima at 606 and 481 nm and molar extinction coefficients ε_M of 163 and 158 $Lmol^{-1}cm^{-1}$, respectively. Below 400 nm, the absorptions gain considerably in intensity, reaching a maximum at 256 (ε_M = 6760 $Lmol^{-1}cm^{-1}$) with shoulders observable on the low-energy side at 329 nm (ε_M = 266 $Lmol^{-1}cm^{-1}$), 292 (ε_M = 662 $Lmol^{-1}cm^{-1}$), and 277 nm (ε_M = 2150 $Lmol^{-1}cm^{-1}$). Based on the calculations, the absorption bands at 606 and 481 nm arise mainly from three $O_2C \rightarrow d_{z^2}$ or $d_{x^2-y^2}$ LMCT (ligand to metal charge transfer) transitions, while the shoulder at 329 nm is ascribed to an *interligand* $O_2C \rightarrow$py transition (Figure S22).[13] In contrast, the spectrum of the reduced complex **1** exhibits considerably stronger absorbing features with maxima found at 838, 667, and 432 nm and molar extinction coefficients of 7050, 3410, and 4070 $Lmol^{-1}cm^{-1}$, respectively.

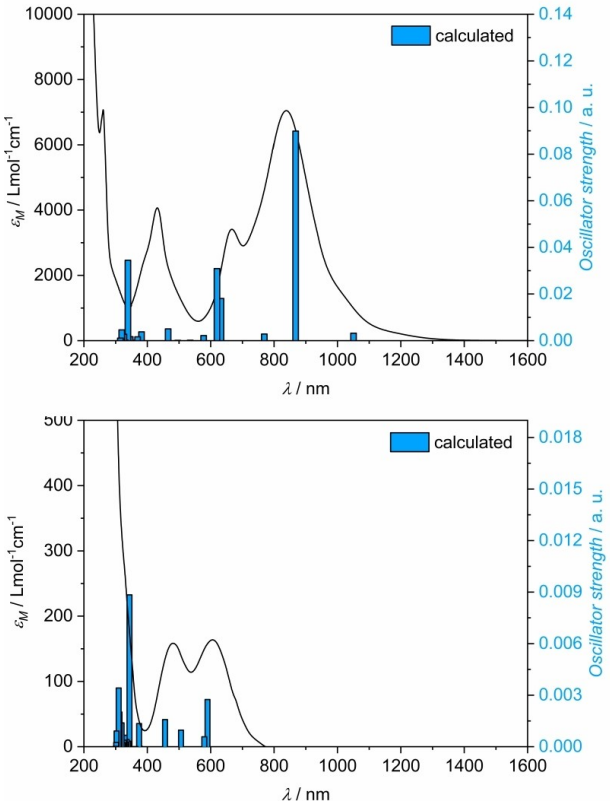

Figure 4. Electronic absorption spectra of **1** (top) and $\mathbf{1}^+$ (bottom) in acetonitrile solutions. The excitations resulting from TD-DFT calculations are inserted as bar charts. The heights of the bars represent the calculated oscillator strengths of the excitations in arbitrary units. A summary of the computed wavelengths and dipole oscillator strengths of the excitations in **1** and $\mathbf{1}^+$.is provided in Table S8 in the Supporting Information.

Based on the calculations, the moderately strong shoulder at 1030 nm and the strong absorption at 838 nm are attributed to *intraligand* py→py transitions within the tetraazamacrocycle (Figure 5), while the higher energy flank of the 838 nm-feature as well as the absorption band around 667 nm arise mainly from various py→d LMCT transitions and, to a lesser extent, from $O_2C \rightarrow$d LMCT transitions with low contributions of a d–d transition (Figure S21).[13] The absorption band at 432 nm with shoulders at 498 and 388 nm has a variety of contributing transitions, among them $O_2C \rightarrow$d LMCT, *intraligand* py→py, and *interligand* $O_2C \rightarrow$py transitions. The finding that the very intense absorption feature between 840 and 1030 nm is almost exclusively related to *intraligand* py→py (β-spin→β-spin) transitions is especially noteworthy to our discussion. These transitions concern only the pyridine units and, therefore, depend crucially on the respective redox state of pyridine moieties. Neutral pyridine units, regardless of which metal ion in which oxidation state they are coordinated to, will not exhibit

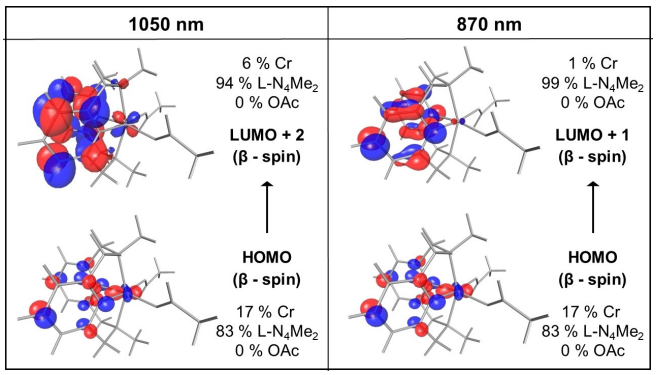

Figure 5. Plot of the canonical molecular orbitals which are mainly involved in the calculated excitations at 1050 and 870 nm for complex **1**. The contributions of the individual components in the complex corresponding to these molecular orbitals are indicated.

such transitions. Therefore, this intensive absorption band unambiguously proves the monoanionic π-radical state of the pyridine units in the coordinated macrocyclic ligand in **1** and can be used as a marker band in future investigations. It is interesting to note that a similarly intense spectroscopic feature at 948 nm has been observed for the in situ prepared complex $[Cr(tpe)_2]^{2+}$, which has also been regarded as a chromium(III) complex containing a coordinated pyridine radical ligand, based on theoretical calculations.[12b]

The DFT investigation was also extended to vibrational spectroscopy. Due to the idealized C_2 symmetry, most vibrational modes occur in pairs where the individual symmetry-related localized vibrations can couple symmetrically or antisymmetrically with each other with respect to the C_2 symmetry operation. A comparison of the intensities of the corresponding symmetric and antisymmetric vibrational modes in the oxidized and the reduced chromium complex (Tables S6 and S7)[13] reveal that some of the antisymmetric vibrations (with respect to the C_2 rotation) are considerably enhanced in the reduced complex compared to the symmetric one. This is related to the fact that, in the reduced macrocyclic ligand, due to the idealized C_2 symmetry of the complex, the unpaired electron residing in a specific antibonding π*-molecular orbital is delocalized over both pyridine rings. Thus, at the equilibrium position of a vibration, two antibonding π*-molecular orbital (π*-MO_{tot}) delocalized over both pyridine rings with one being filled by an electron can be regarded as being constructed from two equally contributing molecular orbitals localized on each of the two pyridine rings (π*-MO_{ind}) by a symmetric and antisymmetric combination. The covalent π-interaction of the antisymmetric π*-MO_{tot} with the d_{xy} orbital of the metal ion (see plot of β-HOMO in Figure 5) lifts the degeneracy of both π*-MO_{tot} and greatly impedes the localization of the unpaired electron on just one of the pyridine units. Any vibrational mode affecting a change in bond length (especially those of the C–N bonds) within a pyridine ring can periodically increase and decrease the energy of the π*-MO_{ind} on each pyridine ring. If a vibration is antisymmetric, the rising and lowering in energy of the individual π*-MO_{ind} contributors localized on each ring will be out-of-phase to each other. Thus, a suitable antisymmetric vibration leads to a periodically occurring alteration of contributions from each localized π*-MO_{ind} (resulting in a break of symmetry) to the delocalized overall π*-MO_{tot} and, thereby, to a transfer of electron population back and forth from one pyridine ring to the other. This, again, renders a huge dipole moment derivative vector (which lies in the CrN_{py2} plane with its orientation perpendicular to the C_2 axis) during a cycle of the vibration and, thereby, to a considerable increase in intensity of the antisymmetric vibration in the IR spectrum. This vibration-induced periodic movement of electron density from one pyridine ring to the other cannot occur during any symmetric vibration because, there, the raising and lowering of the energy of the localized π*-MO_{ind} occur in-phase. In complexes where each of the π-bonding molecular orbitals is occupied by two electrons, this mechanism of increasing the intensity of the antisymmetric vibration relative to the symmetric vibration cannot take place. In order to be actually able to detect the relative increase in intensity of some of the antisymmetric vibrations in **1** compared to those in $\mathbf{1}^+$, an IR-spectroelectrochemical investigation was initiated.

Therefore, a solution of $\mathbf{1}^+$ in deuterated acetonitrile was reduced at an applied constant potential and subsequently reoxidized. The sequence of IR-difference spectra recorded for the reduction and that of the subsequent reoxidation at constant time intervals (Figure S12) indicate the reversibility of the redox processes during the spectroelectrochemical experiment. In Figure 6 a comparison of the difference spectrum after completion of the initial reduction and the corresponding difference spectrum generated from the calculated IR-spectra of **1** and $\mathbf{1}^+$ is displayed.

The calculated difference spectrum nicely reproduces all the features of the experimental spectrum. In general, two types of signals can be distinguished in the difference spectrum. If an IR feature only shifts in energy upon reduction of $\mathbf{1}^+$, but does not change substantially in intensity, the difference spectrum will afford a derivative-shaped signal. One derivative-shaped signal is observed at 1627 (negative component) and 1608 cm^{-1} (positive component) and the other at 1313 (positive component) and 1305 cm^{-1} (negative component). Both derivative-shaped signals arise from energetic shifts of C–O stretching vibrations in the carboxylate units.[25] The change in the redox state of the pyridine units in the *trans* positions to the acetate ligands will somewhat affect the frequency of the vibration, but, to a considerably lesser extent the intensity of carboxylate-based vibrations. In contrast, antisymmetric ring stretching vibrations within the pyridine units gain substantially in intensity in the reduced complex, rendering only positive signals in the difference spectrum. Such signals are observed at 996 and 1574 cm^{-1} in the spectrum in Figure 6. For both vibrations, the corresponding dipole moment derivative vectors are parallel to the line connecting the two pyridine N atoms, consistent with the picture of an electronic charge flowing between the two pyridine units when the geometry moves along the normal coordinate. The broad positive feature in the difference spectrum between 1380 and 1400 cm^{-1} arises from several vibrations which gain considerably in intensity in the

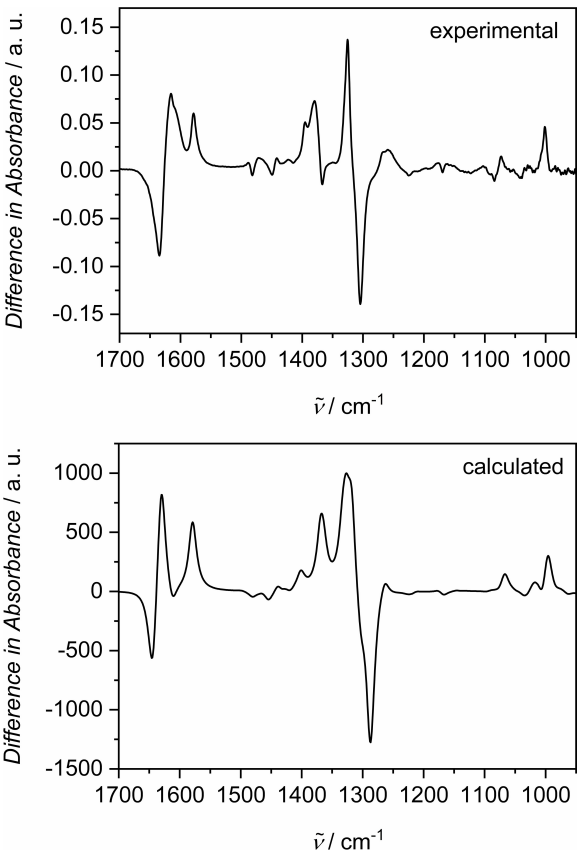

Figure 6. Comparison between the spectroelectrochemical IR-difference spectrum (recorded after 290 s of reduction of a solution of $\mathbf{1}^+$ in MeCN-d_3 at an applied potential of −1.20 V versus an Ag wire; top) and the difference between the calculated IR spectra of **1** and $\mathbf{1}^+$ (bottom). The calculated vibration frequencies were scaled down using a factor of 0.98.

reduced complex. Overall, the impressive agreement between the calculated and the experimental difference spectra provides confidence that the theoretical calculations are correct and, therefore, the electronic ground state of **1** is adequately described by the calculations.

In addition, the strong increase in the intensity of the out-of-phase stretching vibrations of the two pyridine units suggests that, on the quite short time-scale of molecular vibrations, the unpaired electron is delocalized over both pyridine rings. This delocalization is, in our opinion, essential to the stability of the reduced complex; this property eventually allowed us to isolate this complex containing a reduced pyridine radical anion. This is most likely also responsible for the observation that typical reactions of pyridyl radicals (e.g. coupling reactions)[19] have not been detected.

As described in the introduction, the electronic nature of complex **1** could be described either as a chromium(II) complex containing a neutral tetraazamacrocyclic ligand or as a chromium(III) complex with a reduced monoanionic radical ligand. The circumstance that both electronic descriptions share the same spin state and, additionally, that metal-ligand bond lengths would not vary substantially in both extreme descriptions means that any mixture of both depictions could be principally realized as well. Therefore, obtaining the correct description of the electronic state is quite challenging for this type of molecule and cannot be achieved through experimental evidence alone. The results of a carefully executed structural and spectroscopic characterization could be interpreted either way and remain, thereby, inconclusive - if this were the *sole* evidence available. On the other hand, theoretical calculations alone cannot provide an unambiguous answer because states with a different description of the electronic structure could be energetically close (separated only by a few hundreds of cm^{-1}), and computational methods do not have the degree of accuracy needed to determine which one is actually the ground state unless the method has previously been carefully parameterized with a number of well-defined *and* structurally similar model complexes, which are not available here. Therefore, only if the results of theoretical calculations correctly reflect *all* trends of the experimental data obtained by structural analysis *and* various spectroscopic methods, as is the case here, can this constitute convincing and reliable proof for a correct description of the electronic state. In the end, all these efforts leading to the description of complex **1** as chromium(III) complex containing a radical ligand support the coordination chemist's intuition that the ligand field strength of a pseudo-octahedral N_4O_2-donor environment is not sufficient to favour a low-spin chromium(II) state.

Conclusions

In summary, the electronic nature of complex **1** could be unambiguously attributed to a chromium(III) complex containing a reduced monoanionic diazapyridinophane radical ligand by the combination of experimental and theoretical methods. By examining this reduced chromium complex, it has now been clearly established that the previous notion that this type of tetraazamacrocyclic ligand can always be regarded as a redox-inactive "innocent" ligand needs to be revised. In addition to structural analytical methods, spectroscopic tools were identified to unequivocally verify the presence of a reduced diazapyridinophane radical ligand in a complex. It is foreseeable that, with this class of ligands (possibly only after derivatizing the ligand by an introduction of electron-withdrawing substituents at the pyridine ring in order to increase its redox potential), further complexes containing a tetraazamacrocyclic radical ligand could be prepared with metal ions other than chromium.

Nonetheless, obtaining a stable, isolatable (albeit highly oxygen-sensitive) chromium(III) complex with a coordinated monoanionic radical ligand $(L\text{-}N_4Me_2)^{\bullet-}$ was neither anticipated nor planned at the beginning of this study. The uncoordinated macrocycle does not exhibit a reversible or irreversible reduction in the experimentally accessible range of redox potentials in acetonitrile solution. In contrast to aromatic or aliphatic diimines, the reduction of an electronically isolated pyridine ring is considerably more difficult, and the resulting radical pyridine anions are prone to being highly reactive, leading, for example, to ring coupling reactions.[19] Well-defined and structurally characterizable metal complexes with reduced isolated pyridine rings which have been obtained as pure solids

are extremely rare and have been reported, until now, only once with an iron(II) complex.[19] Compound **1** is now the second example for this extremely rare and highly elusive class of compounds.

Another aspect, which should be pointed out when summarizing the scientific significance of our findings, is the feature of the complex that a substitution of the two *cis*-coordinating acetate ligands by (an)other ligand(s) with different ligand field strength and/or metal oxidation state-stabilizing properties can easily be achieved. Thus, complexes with the appropriate composition to enable the observation of temperature-induced changes of electronic states are within synthetic reach. The occurrence of spin-crossover processes has already been reported for a few low-spin chromium(II) complexes.[10,26] In contrast, valence tautomerism has, to best of our knowledge, not yet been established for any chromium complex until now. With the secured identification of the electronic ground state in complex **1** as a chromium(III) ion coordinated to a π-radical, the search for a complex that fills this gap seems to be very promising.

Experimental Section

Synthetic Procedures. Most reagents and reactants were obtained from commercial sources. $[\{Cr(H_2O)\}_2(\mu\text{-}OAc)_4]$ was prepared according to procedures reported in the literature.[27] The macrocyclic ligand L-N_4Me_2 was synthesized employing modified reported methods.[28,29] The anhydrous solvent acetonitrile was dried with CaH_2 and freshly distilled prior to use. Due to the extreme oxygen-sensitivity of the compound $[Cr(L\text{-}N_4Me_2)(OAc)_2]$ (**1**), synthetic procedures need to be performed under a stringent exclusion of oxygen, and the solid must be stored under a nitrogen atmosphere. The solid *crystalline* compound can be handled briefly (less than five minutes) in air (e.g. for the purpose of weighing material or recording an ATR-IR spectrum).

$[Cr(L\text{-}N_4Me_2)(OAc)_2]$ (**1**). Under an atmosphere of nitrogen, solid $[\{Cr(H_2O)\}_2(\mu\text{-}OAc)_4]$ (94 mg, 0.25 mmol) and L-N_4Me_2 (140 mg, 0.52 mmol) were dissolved in absolute acetonitrile (20 mL). After five cycles of heating the stirred reaction mixture to reflux temperatures and cooling it down to room temperature, the volume of the resulting solution was reduced to 10 mL. By diffusing diethylether into the solution, an analytically pure compound $[Cr(L\text{-}N_4Me_2)(OAc)_2]$ could be obtained as deep-green-coloured crystals (164 mg, 0.19 mmol, 76% yield). IR (ATR): $\tilde{\nu}$ = 2912, 2360, 1606, 1574, 1438, 1419, 1361, 1313, 1261, 1164, 1147, 1102, 1069, 996, 953, 931, 880, 851, 769, 754, 709, 646, 613, 522, 476, 465, 440, 427, 402 cm^{-1}. UV/Vis (MeCN): λ_{max} (ε_M) = 1030 (1290, sh), 838 (7050), 667 (3410), 498 (1430, sh), 432 (4070), 388 (2590, sh), 300 (1870, sh), 261 nm (7070 $M^{-1}\cdot cm^{-1}$). MS (ESI) (after oxidation by atmospheric oxygen leading to the monocationic complex) m/z (%): 438.1 (100) $[Cr(L\text{-}N_4Me_2)(OAc)_2]^+$. Elemental analysis calcd for $C_{20}H_{26}CrN_4O_4$: C 54.79, H 5.98, N 12.78, found: C 54.62, H, 6.11, N, 12.72. Conductivity (MeCN, 23.1 °C): Λ_M = 16.51 $\Omega^{-1}\cdot cm^2\cdot mol^{-1}$.

$[Cr(L\text{-}N_4Me_2)(OAc)_2](PF_6)$ (**2**). Under an atmosphere of nitrogen, complex **1** was generated in situ from $[\{Cr(H_2O)\}_2(\mu\text{-}OAc)_4]$ (94 mg, 0.25 mmol) and L-N_4Me_2 (140 mg, 0.52 mmol) in absolute acetonitrile (20 mL) by heating the reaction mixture as described above for the synthesis of **1**. A solution of $[Fe(Cp)_2](PF_6)$ (166 mg, 0.50 mmol) in absolute acetonitrile (15 mL) was added to the solution of complex **1**. Analytically pure, blue crystals were obtained by diffusion of diethylether into the concentrated solution (215.6 mg, 0.18 mmol, 72% yield). IR (ATR): $\tilde{\nu}$ = 3107, 3081, 3009, 2935, 1627, 1610, 1485, 1442, 1411, 1362, 1326, 1305, 1227, 1175, 1083, 1040, 1014, 991, 973, 941, 917, 880, 828, 795, 760, 729, 658, 613, 556, 535, 503, 494, 472 cm^{-1}. UV/Vis (MeCN): λ_{max} (ε_M) = 667 (73, sh), 606 (163), 481 (158), 329 (266, sh), 292 (662, sh), 277 (2150, sh), 265 (5290, sh) 256 nm (6760 $M^{-1}\cdot cm^{-1}$). MS (ESI) m/z (%): 438.1 (100) $[Cr(L\text{-}N_4Me_2)(OAc)_2]^+$. Elemental analysis calcd for $C_{20}H_{26}CrF_6N_4O_4P$: C 41.17, H 4.49, N 9.60, found: C 41.11, H 4.46, N 9.62. Conductivity (MeCN, 22.3 °C): Λ_M = 116.6 $\Omega^{-1}\cdot cm^2\cdot mol^{-1}$.

Methods and Instrumentation

Elemental analyses analyses. *Vario Micro CUBE* by Elementar Analysetechnik GmbH.

Electrospray ionization mass spectrometry. Electrospray ionisation (ESI) mass spectrometer *Expression^L-CMS* from *Advion* using the Advion Mass Express software. The results of the measurements were evaluated with the software program *Advion Data Express* and simulations were carried out with *enviPat Web*.[30]

Conductivity experiments. *SevenEasy conductivity* measuring device and a calibrated *InLab 731* electrode from *Mettler Toledo* using 1 mM solutions in acetonitrile at the temperatures indicated under a nitrogen atmosphere.

Electronic absorption spectroscopy. *Cary 5000 UV/VIS/NIR-spectrophotometer* by Varian in the double beam mode.

Infrared spectroscopy. *Jasco FT/IR-6100* Spectrometer (resolution 4 cm^{-1}). The substances were investigated in their neat form using a *Quest Single Reflection ATR Accessory P/N GS10800* by *Specac*. No frequency-dependent ATR-correction of the intensity was applied.

Spectroelectrochemical infrared investigation. *Perkin–Elmer Spectrum Two FT/IR Spectrometer* using a self-built thin layer reflectance spectroelectrochemical cell, which was constructed according to the design of a cell described in the literature.[31] A Teflon spacer of 0.2 mm thickness was employed to separate the upper PEEK block containing the working electrode from the lower CaF_2 window. A platinum disc electrode (5 mm diameter) was used as the working electrode and reflector of the IR-beam. As a counter electrode, a platinum wire was placed at a distance of 1 cm from the center of the working electrode. This counter electrode was surrounded by a silver wire serving as the reference electrode. The spectroelectrochemical cell was placed on the table top of an *IRUBIS* fixed angle specular reflection accessory which was mounted on a standard FTIR slide mount holder. The measurement was performed on a 0.03 M solution of **2** in deuterated acetonitrile containing 0.1 M tetrabutylammonium hexafluorophosphate as electrolyte. This solution was measured as background so that the subsequent measurements provided difference spectra in absorbance. During the recording of the IR spectra with the program *Spectrum TimeBase 3.1.6.8* from *Perkin Elmer*, a reduction potential of – 1.20 V vs. Ag wire (reference electrode) was applied for 300 s followed by an oxidation potential of - 0.75 V vs. Ag for 300 s using *Potentiostat/Galvanostat Autolab PGSTAT 101* and the software *NOVA 2.1.4* by *Metrohm*. Under these experimental conditions a potential of + 0.41 V vs. Ag was

determined for the ferrocene/ferrocenium redox couple used as internal reference.

Cyclic voltammetric experiments. *Potentiostat/Galvanostat 273 A* by Princeton Applied Research employing a saturated calomel reference electrode (SCE), a platinum foil electrode by Metrohm GmbH as working electrode, and a platinum net as counter electrode. Approximately 10^{-5} moles of sample were dissolved in 10 mL of acetonitrile containing 0.2 molL^{-1} tetrabutylammonium perchlorate (TBAP) as the electrolyte. The measurements were carried out at room temperature under a nitrogen atmosphere in a glovebox. Under these experimental conditions, a potential of +0.45 V vs. SCE was determined for the ferrocene/ferrocenium redox couple used as an internal reference.

Magnetic susceptibilities measurements. *Quantum Design MPMS3 Evercool* SQUID magnetometer capable of varying the magnetic field strength to maximally 7 T. The measurements were carried out at an applied magnetic field of 0.5 T in the DC mode, varying the temperature within the specified temperature range. The samples were packed in gelatine capsules and fixed in a straw serving as a non-magnetic sample holder. The data were corrected for the magnetic moment of the sample holder and the gelatine capsule/VSM powder capsule. In addition, the diamagnetic contributions of the sample were estimated with the formula: $\chi_M\ (dia) = -0.5 \cdot M_{rel} \cdot 10^{-6}$ (with M_{rel}: relative molar mass) and subtracted from the measured data. The magnetic data were fitted using the program *PHI 3.1.5* by the Chilton group.[32]

Determination of the magnetic susceptibilities of solutions. The magnetic susceptibilities of solutions were determined by Evans method.[23] using an *Avance I* (600 MHz) NMR spectrometer by Bruker. For this purpose, NMR spectra of 32 mM solutions of **1** in deuterated acetonitrile in a coaxial NMR tube (using a pure oxygen-free sample of the deuterated solvent in the inner tubing) were measured, varying the temperature from 233 to 348 K. The magnetic data were corrected for the diamagnetic contributions of the sample. In addition, the data were subjected to a density correction of the solvent with the formula: $d_t = [d_s + 10^{-3}\ \alpha(t\text{-}t_s) + 10^{-6}\ \beta(t\text{-}t_s)^2 + 10^{-9}\ \gamma(t\text{-}t_s)^3]$ (with: $t_s = 0\,^{\circ}C$, $d_s = 0.8035$, $\alpha = -1.055$, $\beta = -0.138$, $\gamma = -6$).[33]

X-ray diffraction data structure analyses. *Gemini S Ultra* by Rigaku Oxford Diffraction, equipped with a molybdenum and a copper radiation source and a low-temperature control device. Absorption correction with CrysAlis Pro 1.171.38.41 and 1.171.40.67a. Structure solution and refinement: SHELXS-2014 and SHELXL-2014.[34] More detailed information is given in the corresponding sections of the Supporting Information focusing on the structural characterization of the respective complexes. Deposition numbers 2231890 (for **1**) and 2231889 (for **2**) contain the supplementary crystallographic data for this paper. These data are provided free of charge by the joint Cambridge Crystallographic Data Centre and Fachinformationszentrum Karlsruhe Access Structures service.

Density functional calculations were performed using the program package *Turbomole*,[16] applying the B3LYP[17] functional in combination with the def2-TZVP[18] basis set.

More detailed information on the instrumentation as well as the experiments are provided in the Supporting Information.

Deposition Number(s) 2231890 (for 1), 2231889 (for 2) contain(s) the supplementary crystallographic data for this paper. These data are provided free of charge by the joint Cambridge Crystallographic Data Centre and Fachinformationszentrum Karlsruhe Access Structures service.

Supporting Information

Additional references cited within the Supporting Information.

Acknowledgements

We gratefully acknowledge the support by the Deutsche Forschungsgemeinschaft (DFG) (SFB-TRR-88 3MET and INST 248/266-1 FUGG) as well as by the University of Kaiserslautern. Open Access funding enabled and organized by Projekt DEAL.

Conflict of Interests

The authors declare no conflict of interest.

Data Availability Statement

The data that support the findings of this study are available in the supplementary material of this article.

Keywords: chromium · electronic structure · pyridine radical anion · π-radical ligand · tetraazamacrocyclic ligand

[1] a) N. Panza, G. Tseberlidis, A. Caselli, R. Vincente, *Dalton Trans.* **2022**, *51*, 10635; b) F. G. Doro, K. Q. Ferreira, Z. N. da Rocha, G. F. Caramori, A. J. Gomes, E. Tfouni, *Coord. Chem. Rev.* **2016**, *306*, 652; c) N. F. Curtis, in *Comprehensive Coordination Chemistry. From Biology to Nanotechnology. Volume 1 Fundamentals: Ligands, Complexes, Synthesis, Purification, and Structure* (Eds.: J. A. McCleverty, T. J. Meyer), Elsevier, Oxford, **2004**, pp. 447–474.

[2] a) E. Le Saux, E. Georgiou, I. A. Dmitriev, W. C. Hartley, P. Melchiorre, *J. Am. Chem. Soc.* **2023**, *145*, 47; b) L. Meites, P. Zuman, W. J. Scott, B. H. Campbell, A. M. Kardos, *Electrochemical Data, Part 1 Volume A*, John Wiley, New York, **1974**, and references therein.

[3] a) W. O. Koch, H.-J. Krüger, *Angew. Chem. Int. Ed.* **1995**, *34*, 2671; *Angew. Chem.* **1995**, *107*, 2928; b) E. Dobbelaar, C. Rauber, T. Bonck, H. Kelm, M. Schmitz, M. E. de Wall Malefijt, J. E. M. N. Klein, H.-J. Krüger, *J. Am. Chem. Soc.* **2021**, *143*, 13145.

[4] a) H.-J. Krüger, *Coord. Chem. Rev.* **2009**, *253*, 2450; b) F. Rupp, K. Chevalier, M. Graf, M. Schmitz, H. Kelm, A. Grün, M. Zimmer, M. Gerhards, C. van Wüllen, H.-J. Krüger, R. Diller, *Chem. Eur. J.* **2016**, *23*, 2119; c) M. Graf, G. Wolmershäuser, H. Kelm, S. Demeschko, F. Meyer, H.-J. Krüger, *Angew. Chem. Int. Ed.* **2010**, *49*, 950; *Angew. Chem.* **2010**, *122*, 962; d) C. Metzger, R. Dolai, S. Reh, H. Kelm, M. Schmitz, B. Oelkers, M. Sawall, K. Neymeyr, H.-J. Krüger, *Chem. Eur. J.* **2023**, *29*, e202300091.

[5] F. S. Menges, S. M. Craig, N. Tötsch, A. Bloomfield, S. Ghosh, H.-J. Krüger, M. A. Johnson, *Angew. Chem. Int. Ed.* **2016**, *55*, 1282; *Angew. Chem.* **2016**, *128*, 1304.

[6] P. A. Lay, A. Levina, in *Comprehensive Coordination Chemistry Vol. 4* Constable, *Comprehensive Coordination Chemistry II. From Biology to*

Nanotechnology. Volume 4 Transition Metal Groups 3–6 (Eds.: J. A. McCleverty, T. J. Meyer), Elsevier, Oxford, **2004**, pp. 313–413.
[7] C. C. Scarborough, S. Sproules, T. Weyhermüller, S. DeBeer, K. Wieghardt, *Inorg. Chem.* **2011**, *50*, 12446.
[8] a) C. C. Scarborough, K. M. Lancaster, S. DeBeer, T. Weyhermüller, S. Sproules, K. Wieghardt, *Inorg. Chem.* **2012**, *51*, 3718; b) M. Wang, J. England, T. Weyhermüller, S.-L. Kokatam, C. J. Pollock, S. DeBeer, J. Shen, G. P. A. Yap, K. H. Theopold, K. Wieghardt, *Inorg. Chem.* **2013**, *52*, 4472; c) W. Zhou, A. N. Desnoyer, J. A. Bailey, B. O. Patrick, K. M. Smith, *Inorg. Chem.* **2013**, *52*, 2271; d) B. E. Olafsen, G. V. Crescenzo, L. P. Moisey, B. O. Patrick, K. M. Smith, *Inorg. Chem.* **2018**, *57*, 9611; e) S. Joy, P. Pal, T. K. Mondal, G. B. Talapatra, S. Goswami, *Chem. Eur. J.* **2012**, *18*, 1761; f) A. S. Gowda, J. L. Petersen, C. Milsmann, *Inorg. Chem.* **2018**, *57*, 1919; g) J. A. DeGayner, I.-R. Jeon, T. D. Harris, *Chem. Sci.* **2015**, *6*, 6639; h) G. Leone, E. Groppo, G. Zanchin, G. A. Martino, A. Piovano, F. Bertini, J. Martí-Rujas, E. Parisini, G. Ricci, *Organometallics* **2018**, *37*, 4827.
[9] C. C. Scarborough, S. Sproules, C. J. Doonan, K. S. Hagen, T. Weyhermüller, K. Wieghardt, *Inorg. Chem.* **2012**, *51*, 6969.
[10] P. M. Becker, C. Förster, L. M. Carrella, P. Boden, D. Hunger, J. van Slageren, M. Gerhards, E. Rentschler, K. Heinze, *Chem. Eur. J.* **2020**, *26*, 7199.
[11] S. Otto, M. Grabolle, C. Förster, C. Kreitner, U. Resch-Genger, K. Heinze, *Angew. Chem. Int. Ed.* **2015**, *54*, 11572; *Angew. Chem.* **2015**, *127*, 11735.
[12] a) F. Reichenauer, C. Wang, C. Förster, P. Boden, N. Ugur, R. Baez-Cruz, J. Kalmbach, L. M. Carrella, E. Rentschler, C. Ramanan, G. Niedner-Schatteburg, M. Gerhards, M. Seitz, U. Resch-Genger, K. Heinze, *J. Am. Chem. Soc.* **2021**, *143*, 11843; b) S. Treiling, C. Wang, C. Förster, F. Reichenauer, J. Kalmbach, P. Boden, J. P. Harris, L. M. Carrella, E. Rentschler, U. Resch-Genger, C. Reber, M. Seitz, M. Gerhards, K. Heinze, *Angew. Chem. Int. Ed.* **2019**, *58*, 18075; *Angew. Chem.* **2019**, *131*, 18243.
[13] Further details are found in the Supporting Information.
[14] Considering that Heinze et al. reported spin crossover properties for the complex $[Cr(ddpd)_2]^{2+}$ with an CrN_6 coordination sphere[10] and applying basic concepts of coordination chemistry, the change to a CrN_4O_2 coordination unit in **1** is expected to decrease the ligand field splitting to such an extent that the presence of a low-spin chromium(II) state in **1** can safely be considered unlikely.
[15] The z-axis is defined to be colinear to the N_{amine}–N_{amine} axis, while the x- and y-axes are placed along the Cr–N_{py} bonds. Note the definition of coordination axis for the discussion of molecular orbitals is different to that used in the discussion of the vibrational properties where in the idealized C_2 symmetry the z-axis lies along the bisector of the N_{py}–Cr–N_{py} bond angle.
[16] a) S. G. Balasubramani, G. P. Chen, S. Coriani, M. Diedenhofen, M. S. Frank, Y. J. Franzke, F. Furche, R. Grotjahn, M. E. Harding, C. Hättig, et al., *J. Chem. Phys.* **2020**, *152*, 184107; b) R. Ahlrichs, M. Bär, M. Häser, H. Horn, C. Kölmel, *Chem. Phys. Lett.* **1989**, *162*, 165.
[17] a) P. J. Stephens, F. J. Devlin, C. F. Chabalowski, M. J. Frisch, *J. Phys. Chem.* **1994**, *98*, 11623; b) A. D. Becke, *J. Chem. Phys.* **1993**, *98*, 5648.
[18] F. Weigend, R. Ahlrichs, *Phys. Chem. Chem. Phys.* **2005**, *7*, 3297.
[19] T. R. Dugan, E. Bill, K. C. MacLeod, G. J. Christian, R. E. Cowley, W. W. Brennessel, S. Ye, F. Neese, P. L. Holland, *J. Am. Chem. Soc.* **2012**, *134*, 20352.
[20] neutral pyridine: C–N: 1.348 Å, C–C_{adj}: 1.386 Å and C–C_{dis}: 1.391 Å; radical pyridine anion: C–N: 1.370 Å, C–C_{adj}: 1.373 Å and C–C_{dis}: 1.400 Å.
[21] a) D. P. Rillema, D. S. Jones, C. Woods, H. A. Levy, *Inorg. Chem.* **1992**, *31*, 2935; b) M. Biner, H. B. Buergi, A. Ludi, C. Roehr, *J. Am. Chem. Soc.* **1992**, *114*, 5197.
[22] In contrast to the complexes **1** and $\mathbf{1}^+$, an increase of the Cr–N_{py} bond lengths is found in theoretical calculations on the chromium complexes $[Cr(ddpd)_2]^n$ ($n = 2+, 3+$)[10,11] where the reduced complex is described as a low-spin chromium(II) complex. It appears that, in these complexes, the lengthening of the Cr-N_{py} bond arises from the increase of the ionic radius of the chromium ion due to its lower oxidation state, outweighing the effect of an increase in π-back bonding due to the greater electron richness of the more reduced metal ion.
[23] a) D. F. Evans, *J. Chem. Soc.* **1959**, 2003; b) E. M. Schubert, *J. Chem. Educ.* **1992**, *69*, 62; c) D. H. Grant, *J. Chem. Educ.* **1995**, *72*, 39; d) C. Piguet, *J. Chem. Educ.* **1997**, *74*, 815.
[24] A. Dreuw, J. L. Weisman, M. Head-Gordon, *J. Chem. Phys.* **2003**, *119*, 2943.
[25] K. Nakamoto, *Infrared and Raman Spectra of Inorganic and Coordination Compounds, Fifth Edition, Part B: Applications in Coordination, Organometallic and Bioinorganic Chemistry*, Wiley Interscience, New York, **1997**, 57–78.
[26] a) D. M. Halepoto, D. G. L. Holt, L. F. Larkworthy, G. J. Leigh, D. C. Povey, G. W. Smith, *J. Chem. Soc., Chem. Commun.* **1989**, 1322; b) M. Sorai, Y. Yumoto, D. M. Halepoto, L. F. Larkworthy, *J. Phys. Chem. Solids* **1993**, *54*, 421; c) H. Sitzmann, M. Schär, E. Dormann, M. Kelemen, *Z. Anorg. Allg. Chem.* **1997**, *623*, 1850; d) M. B. Meredith, J. A. Crisp, E. D. Brady, T. P. Hanusa, G. T. Yee, M. Pink, W. W. Brennessel, V. G. Young, *Organometallics* **2008**, *27*, 5464; e) A. K. Hughes, V. J. Murphy, D. O'Hare, *J. Chem. Soc., Chem. Commun.* **1994**, 163.
[27] L. R. Ocone, B. P. Block, J. P. Collman, D. A. Buckingham, *Inorg. Synth.* **1966**, *8*, 125.
[28] B. Alpha, E. Anklam, R. Deschenaux, J.-M. Lehn, M. Pietraskiewiez, *Helv. Chim. Acta* **1988**, *71*, 1042.
[29] F. Bottino, M. Di Grazia, P. Finocchiaro, F. R. Fronczek, A. Mamo, S. Pappalardo, *J. Org. Chem.* **1988**, *53*, 3521.
[30] M. Loos, C. Gerber, F. Corona, J. Hollender, H. Singer, *Anal. Chem.* **2015**, *87*, 5738.
[31] I. S. Zavarine, C. P. Kubiak, *J. Electroanal. Chem.* **2001**, *495*, 106.
[32] N. F. Chilton, R. P. Anderson, L. D. Turner, A. Soncini, K. S. Murray, *J. Comput. Chem.* **2013**, *34*, 1164.
[33] R. F. Brunel, K. van Bibber, in *International Critical Tables of Numerical Data, Physics, Chemistry and Technology - Volume III*, (Ed.: E. W. Washburn), McGraw-Hill, New York, **1928**, pp. 27–35.
[34] a) G. M. Sheldrick, *Acta Crystallogr. Sect. C* **2015**, *71*, 3; b) G. M. Sheldrick, *Acta Cryst. Sect. A, Found. Crystallogr.* **2008**, *64*, 112.
[35] P. Deglmann, F. Furche, R. Ahlrichs, *Chem. Phys. Lett.* **2002**, *362*, 511.
[36] a) "Computational Chemistry Comparison and Benchmark DataBase", can be found under https://cccbdb.nist.gov/vibscalejust.asp; b) M. P. Andersson, P. Uvdal, *J. Phys. Chem.* **2005**, *109*, 2937.
[37] R. Bauernschmitt, R. Ahlrichs, *Chem. Phys. Lett.* **1996**, *256*, 454.

Manuscript received: April 6, 2023
Accepted manuscript online: October 30, 2023
Version of record online: December 4, 2023